Transactions of Materials Research 1 (2025) 100009

Contents lists available at ScienceDirect

Transactions of Materials Research

journal homepage: www.sciencedirect.com/journal/transactions-of-materials-research

Enhanced in-plane polarization in two-dimensional $GaInS_3$ via strain engineering for self-powered photodetector

Zongdong Sun [a], Jie Liu [a], Na Zhang [a], Wanfu Shen [b], Chunguang Hu [b], Liang Li [c], Feng Yan [d], Fangfang Xia [a], Huiqiao Li [a], Yuan Li [a], Tianyou Zhai [a,e,f,*]

[a] State Key Laboratory of Materials Processing and Die & Mould Technology, School of Materials Science and Engineering, Huazhong University of Science and Technology (HUST), Wuhan, 430074, China
[b] State Key Laboratory of Precision Measuring Technology and Instruments, Tianjin University, Tianjin, 300072, China
[c] Key Laboratory of Materials Physics, Anhui Key Laboratory of Nanomaterials and Nanotechnology, Institute of Solid State Physics, Hefei Institutes of Physical Science, Chinese Academy of Sciences, Hefei, 230031, China
[d] Department of Applied Physics, Research Institute of Intelligent Wearable Systems, The Hong Kong Polytechnic University, Kowloon, 999077, Hong Kong, China
[e] Research Institute of Huazhong University of Science and Technology in Shenzhen, Shenzhen, 518057, China
[f] Optics Valley Laboratory, Wuhan, 430074, China

ARTICLE INFO

Keywords:
Two-dimensional materials
Self-powered photodetector
Polarization
Strain engineering
In-plane anisotropy

ABSTRACT

Self-powered two-dimensional (2D) polarization-sensitive photodetectors have propelled the advancement of the next-generation optoelectronics. However, currently such devices mainly depend on the stacking of multiple 2D heterojunctions to realize this function, which demands precise operational procedures and strict band alignment. Herein, we present the achievement of self-powered polarization photodetection in 2D $GaInS_3$ via strain engineering. This primarily depends on the intrinsic in-plane anisotropic structure and internal spontaneous polarization of 2D $GaInS_3$. Remarkedly, the strained $GaInS_3$ devices exhibit superior optoelectronic performance with a high on/off ratio ($>10^4$), and large anisotropy ratio (~5.4). Furthermore, the strained device can achieve self-powered high-resolution polarization imaging. This work offers a guideline valuable for developing high-performance 2D self-powered polarization photodetectors.

1. Introduction

Polarization-sensitive photodetectors, under their ability to sense and identify objects efficiently in complex environments, have extensive applications in communication remote-sensing, scanning imaging, machine vision, and others [1–5]. Traditional polarization photodetectors with redundant optical components and low sensitivity are unable to meet the increasing demand for device miniaturization and multifunction integration [6]. Two-dimensional (2D) materials have undergone extensive research in optoelectronics owing to their distinctive optical and electrical properties [7–9]. Among them, a class of 2D materials with in-plane anisotropy exhibits significant application prospects in polarization-sensitive photodetection [10–12].

With the ongoing advancement and investigation of various 2D anisotropic materials, it has become feasible to engineer distinct types of heterojunctions through bandgap engineering to realize self-powered polarized photodetectors. This approach not only reduces power consumption but also simplifies the device configuration [13–16]. However, this also requires strict band alignment and complex precision operation procedures. Although the bulk photovoltaic effect of 2D ferroelectric materials is being recognized, the highly symmetric in-plane crystal structures of In_2Se_3 [17] and $CuInP_2S_6$ [18] fail to show strong in-plane anisotropic optical characteristics, due to the fact that flexible 2D materials have a high deformative tolerance [19] and by applying strain engineering [20] the in-plane polarization can be significantly enhanced to achieve the bulk photovoltaic effect [21–23]. However, this remains elusive for realizing self-powered polarization-sensitive optoelectronic detectors.

In this work, we propose that strain engineering can enhance the spontaneous polarization of $GaInS_3$ to accomplish the self-powered polarization-sensitive optoelectronic function. The anisotropy and dipole polarization in-plane of 2D $GaInS_3$ are characterized and analyzed by

* Corresponding author. State Key Laboratory of Materials Processing and Die & Mould Technology, School of Materials Science and Engineering, Huazhong University of Science and Technology (HUST), Wuhan, 430074, China.
E-mail address: zhaity@hust.edu.cn (T. Zhai).

https://doi.org/10.1016/j.tramat.2025.100009
Received 21 March 2025; Received in revised form 4 April 2025; Accepted 5 April 2025
Available online 5 April 2025

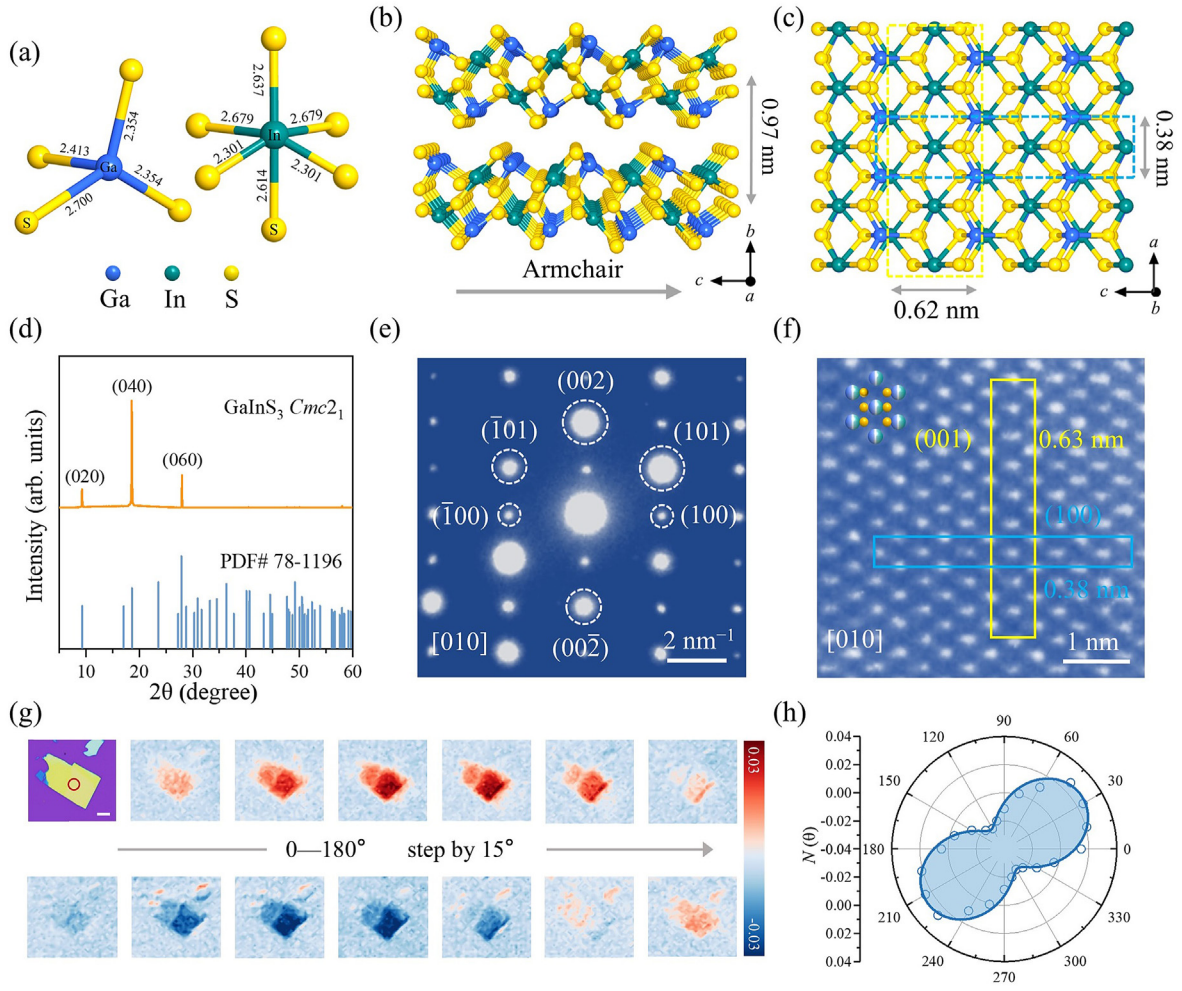

Fig. 1. Structural and anisotropic characterizations of $GaInS_3$. (a) The bond geometric diagram of the GaS_4 tetrahedron and the InS_6 octahedron. Bond length units: Å. The inset shows the single crystals of $GaInS_3$. (b, c) Side and top views of the $GaInS_3$ structure. The *c*-axis is defined as the Armchair direction, and the interlayer spacing is 0.97 nm. The lateral and vertical distances of the Ga/In atomic columns are marked by the orange and blue dashed frames, respectively. (d) Experimental and calculated XRD patterns of $GaInS_3$. (e) The corresponding SAED pattern of $GaInS_3$ along the [010] direction. (f) High-resolution TEM of 2D $GaInS_3$. The blue and green double-color balls denote Ga/In atoms, and the yellow balls represent S atoms. The distances of Ga/In atoms along the AC and ZZ directions are represented by light blue and yellow frames, respectively. (g) The angle-resolved ADRDS mapping, scale bar: 10 μm. (h) Polar plot of ADRDS intensities of $GaInS_3$ with the intensities extracted from the red circle mark on the $GaInS_3$ nanosheets in Figure. g.

angle-resolved polarization Raman spectra (ARPRS), angle-dependent reflectance difference spectroscopy (ADRDS), and second-harmonic generation (SHG), and piezo-response microscopy (PFM), respectively. The strained device is obtained by transferring $GaInS_3$ nanosheets onto the prefabricated bottom Au electrodes through the dry transfer method. Under 365 nm wavelength illumination, the strained $GaInS_3$ device demonstrates a remarkable bulk photovoltaic response, and the open-circuit current (I_{oc}) can be modulated through the crystal orientation and strain coefficient. The self-powered detector manifests outstanding photoelectric properties, a high on/off ratio ($I_{on/off} > 10^4$), appropriate responsivity ($R \sim 85$ mA W^{-1}) and considerable polarization ratio (PR ~ 5.4). Additionally, self-powered polarization imaging is employed to verify the reliability of the strained device. This work presents a new approach in exploration of high-performance 2D self-powered polarization-sensitive photodetectors.

2. Experimental

2.1. Materials preparation and characterizations

$GaInS_3$ bulk single crystals were obtained by employing the chemical vapor transport (CVT) method [24]. Nanosheets of $GaInS_3$ were prepared from the bulks by mechanical exfoliation and transferred onto arbitrary substrates. The morphology and thickness of the as-prepared nanoplates were observed by means of an optical microscope (Olympus, BX51) and an atomic force microscope (AFM, Bruke, Dimension Icon), respectively. The phase and composition of the nanosheets were investigated and characterized by an X-ray diffractometer (XRD, Burker, D2 Phaser) and a scan scanning electron microscope (SEM) equipped with energy dispersive spectrometer (EDS, Quanta 650 FEG, FEI). Selected area electron diffraction (SAED) and high-resolution transmission electron microscopy (HRTEM) are acquired by means of a transmission electron microscope (FEI, Tecnai G2 F30). The angle-resolved polarization Raman spectra were performed by using a confocal microscope spectrometer (WITec, Alpha300RS+) with a 40 × objective lens and a 532 nm laser source. For angle-dependent reflection difference spectroscopy (ADRDS), the polarization direction of the linearly polarized incident light is modulated by a polarizer and a liquid crystal variable delay (Thorlabs, LCC1113-A). After traversing the lens and bandpass filter, the reflected light signal from the $GaInS_3$ sample is captured by a charge-coupled device (Apogee, AltaU2).

2.2. SHG and PFM measurements

The SHG measurements were performed using a Ti:Sapphire

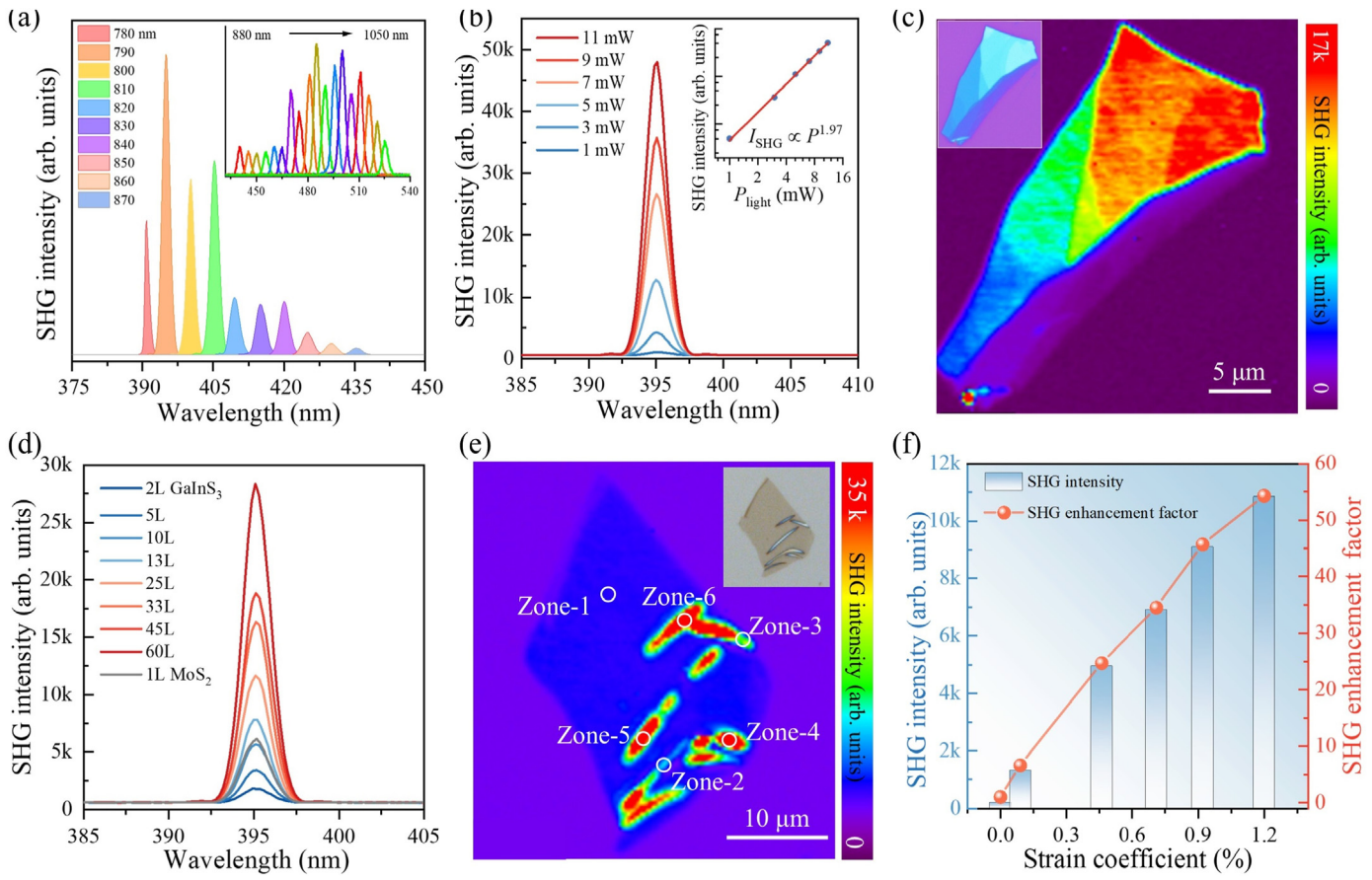

Fig. 2. SHG characterizations of 2D $GaInS_3$. (a) Wavelength-dependent SHG response from 780 to 1050 nm. (b) Power-dependent SHG intensity and fitting curve at 790 nm laser with the power range of 1–11 mW. (c) SHG intensity mapping of multi-layer $GaInS_3$, insert picture: microscopic morphology of $GaInS_3$, the thickness ranges from 5L to 32L. (d) Layer-dependent SHG intensities curve. (e) SHG intensity mapping of strained $GaInS_3$. The white circles denote the regions where different strain coefficients were extracted, respectively. The inset is optical image strained $GaInS_3$, the thickness of the flat area is only 15 nm, and the thickness of the fold area can reach 200 nm. (f) The histogram of the $GaInS_3$ SHG intensity under different strain coefficients and the line graph of the SHG enhancement factor for statistics.

femtosecond laser (140 fs, 80 MHz) with an excitation wavelength range of 780–1050 nm. The sample surface was focused by a confocal microscope spectrometer (WITec, Alpha300RS+) equipped with a 40 × objective lens. A linear analyzer was installed in front of the detector to collect SHG signals in parallel and vertical configurations. The half-wave plate was placed in the optical path to regulate the polarized direction. The lateral piezoelectric response was measured using a piezoelectric force microscope (PFM, Oxford Instruments Asylum Research, Jupiter XR). In the PFM characterization, a conductive probe coated with Pt/Ir, having a force constant of 2.8 N/m, was employed, and an AC bias voltage within the range of 1–4 V was applied. To minimize the interference of surface charges, the exfoliated nanosheets were transferred onto a conductive substrate (silicon substrate) and grounded.

2.3. Devices fabrication and characterizations

The bottom electrode patterns were fabricated on a 300 nm SiO_2/Si substrate via electron beam lithography (EBL, Raith GmbH, ELPHY Plus) and the electrodes (150−200 nm Au) were deposited through thermal evaporation (Angstrom Engineering, Nexdep). $GaInS_3$ nanoflakes on polydimethylsiloxane (PDMS) were determined to have a crystal orientation by polarized Raman or SHG, and then transferred to bottom electrode using a transfer platform. The electrical measurements of the device were carried out through a probe station (Lake Shore, TTPX) equipped with a semiconductor analyzer (Keithley, B1500A), and the photoelectric response was tested by an external 365 nm wavelength laser (Thorlabs, M365FP1).

3. Results and discussion

$GaInS_3$ crystallizes in the orthorhombic *mm*2 point group (space group $Cmc2_1$), which is a typical non-centrosymmetric structure. Spontaneous polarization may exist within this crystal structure, which is expected to find applications in fields such as nonlinear optics and piezoelectricity [25,26]. As depicted in Fig. 1a, $GaInS_3$ encompasses two structural units, namely the GaS_4 tetrahedron and the InS_6 octahedron. In light of the bond lengths presented in the polyhedra, the M−S bonds within these two polyhedra are non-equivalent, suggesting that each polyhedron is highly distorted. The coordination geometry is shown in Fig. S1 in the Supplementary materials, with each unit being coordinated to the surrounding polyhedra through edge-sharing and corner-sharing, respectively. Each polyhedron of GaS_4 and InS_6 constitutes a 1D chain-like structure and a 2D planar structure via corner sharing and edge sharing along the *a*-axis (Figs. S2a and b), respectively. These two structures are interlaced along the *ac*-plane to jointly form a 2D $GaInS_3$ structure. Owing to the arrangement of the distorted polyhedra, the $GaInS_3$ structure presents both anisotropic and spontaneous polarization characteristics. Therefore, the low-symmetry in-plane structure of $GaInS_3$ results in Armchair (AC) and zigzag (ZZ) structural features along the *c*-axis and *a*-axis (Fig. 1b and c), respectively. High-quality $GaInS_3$ plate-shaped single crystals (Fig. S3a) can be prepared by the CVT method, and their distinct layered nature can be observed through SEM (Fig. S3b). Bulks $GaInS_3$ can be easily prepared into single or few-layered nanosheets by mechanical exfoliation (Fig. S3c). According to the EDS results, the elemental composition of the single crystal meets the

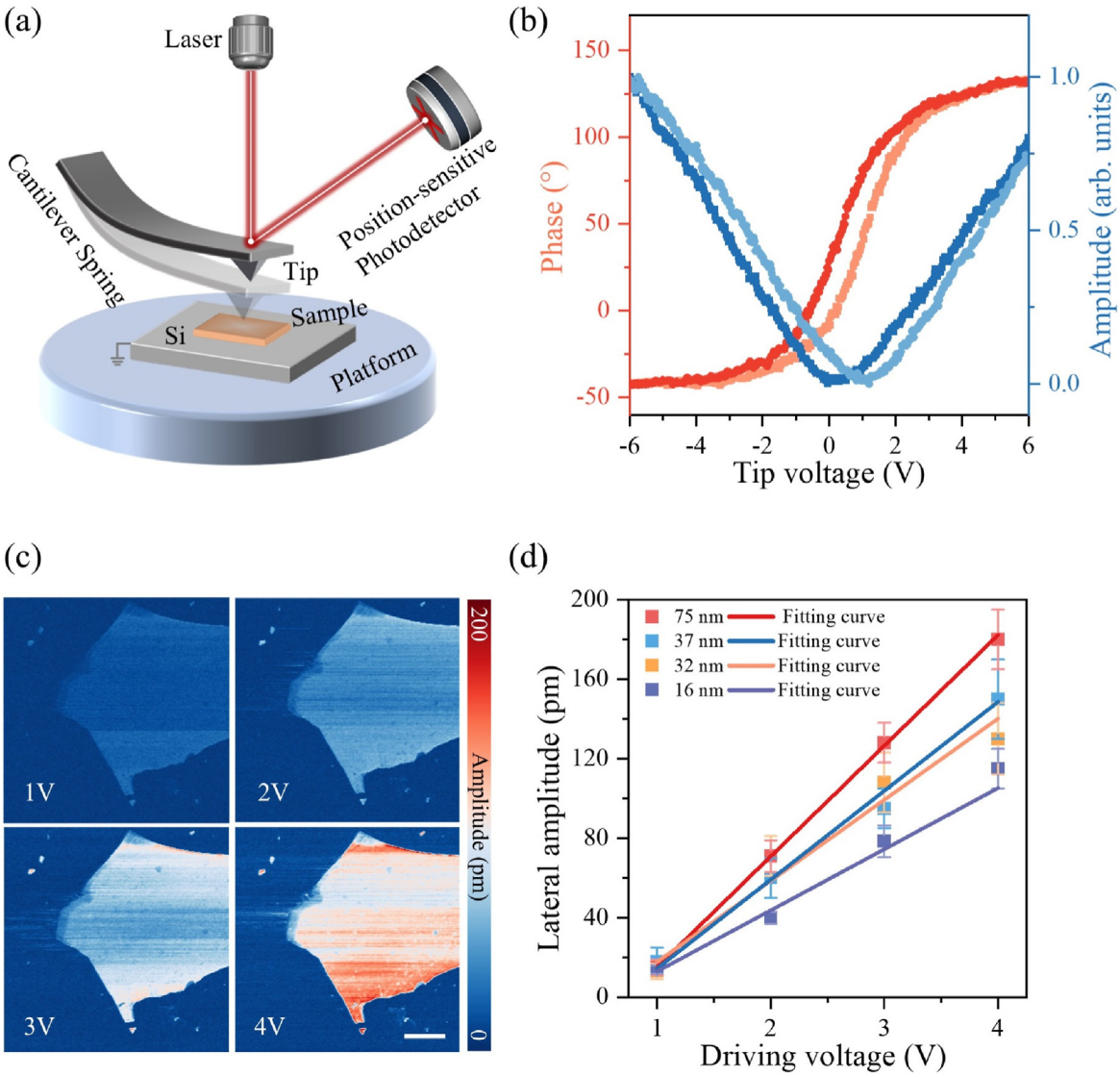

Fig. 3. Characterizations of in-plane piezoelectricity of 2D $GaInS_3$. (a) Schematic of the PFM configuration. (b) The in-plane PFM phase and amplitude curves. (c) The voltage-dependent lateral PFM amplitude mapping. (d) The extracted driving voltage-dependent amplitude response curves for different thicknesses of $GaInS_3$.

chemical stoichiometry (Fig. S4a), and the mapping also indicates a uniform distribution of elements (Fig. S4b). The XRD peaks (Fig. 1d) of the nanosheets match well with the standard card (PDF-78-1196), pointing that the crystals prepared are orthorhombic $GaInS_3$. Moreover, the single-oriented XRD peaks [010] correspond to the *ac*-plane in the $GaInS_3$ structure (Fig. 1c). The phase and fine structure of the as-prepared nanoflakes were further confirmed by TEM. According to the SAED (Fig. 1d), the corresponding spots verified to be along the [010] crystallographic direction. The bright diffraction spots in the HRTEM pattern (Fig. 1f) correspond to Ga/In atomic columns. Their corresponding (001) and (100) faces match with the distances between the AC and ZZ-direction Ga/In atomic columns (Fig. 1c), respectively.

Angle-resolved polarized Raman spectroscopy serves as a favorable characterization means for analyzing the phonon vibration modes and structural orientations of 2D materials [27]. As shown in Figs. S5a and b, the Raman peak intensity of the $GaInS_3$ exhibits a clear angle-dependent relation at the parallel configuration. The Raman intensities extracted from the two positions (104 and 383 cm^{-1}) are listed in polar plots (Figs. S5c and d), and through fitting analysis, they are identified as A1 modes with the strongest peak position in the AC direction. The optical in-plane anisotropy of $GaInS_3$ is further confirmed by ADRDS. With a step of 15°, the ADRDS mapping of $GaInS_3$ nanoflakes within the range of 0–180° is depicted in Fig. 1g. The contrast of the sample undergoes significant variations in accordance with the angle, attaining a maximum reflectance within the range of 30–45°, whereas the isotropic SiO_2 substrate exhibits no change in contrast. The polar plot of the angle-dependent reflectance difference (*N*) is shown in Fig. 1h, and the fitting results reveal a clear periodic feature of the bipolar leaf. These results not only prove the significant anisotropy of the reflectivity in 2D $GaInS_3$, but also provide a reference for quickly identifying the orientation.

SHG is profoundly dependent on the crystal symmetry of the materials, specifically established in the structure of symmetry breaking. Currently, SHG has evolved into a prevalent and effective approach for analyzing the symmetry, crystal orientation, internal defects, etc. [28–30]. An in-depth SHG investigation of 2D $GaInS_3$ enables further symmetry analysis within its structure. To select the appropriate laser excitation wavelength, the wavelength-dependent SHG intensity is presented in Fig. 2a. The results indicate that $GaInS_3$ possesses a wide-band (excitation wavelength: 780–1050 nm) SHG response and the strongest SHG signal intensity under 790 nm excitation. To investigate the NLO mechanism of $GaInS_3$, the correlation between the excitation laser power and the SHG intensity was established under a 790 nm laser. As shown in Fig. 2b, the SHG intensity increases with the augment of the incident

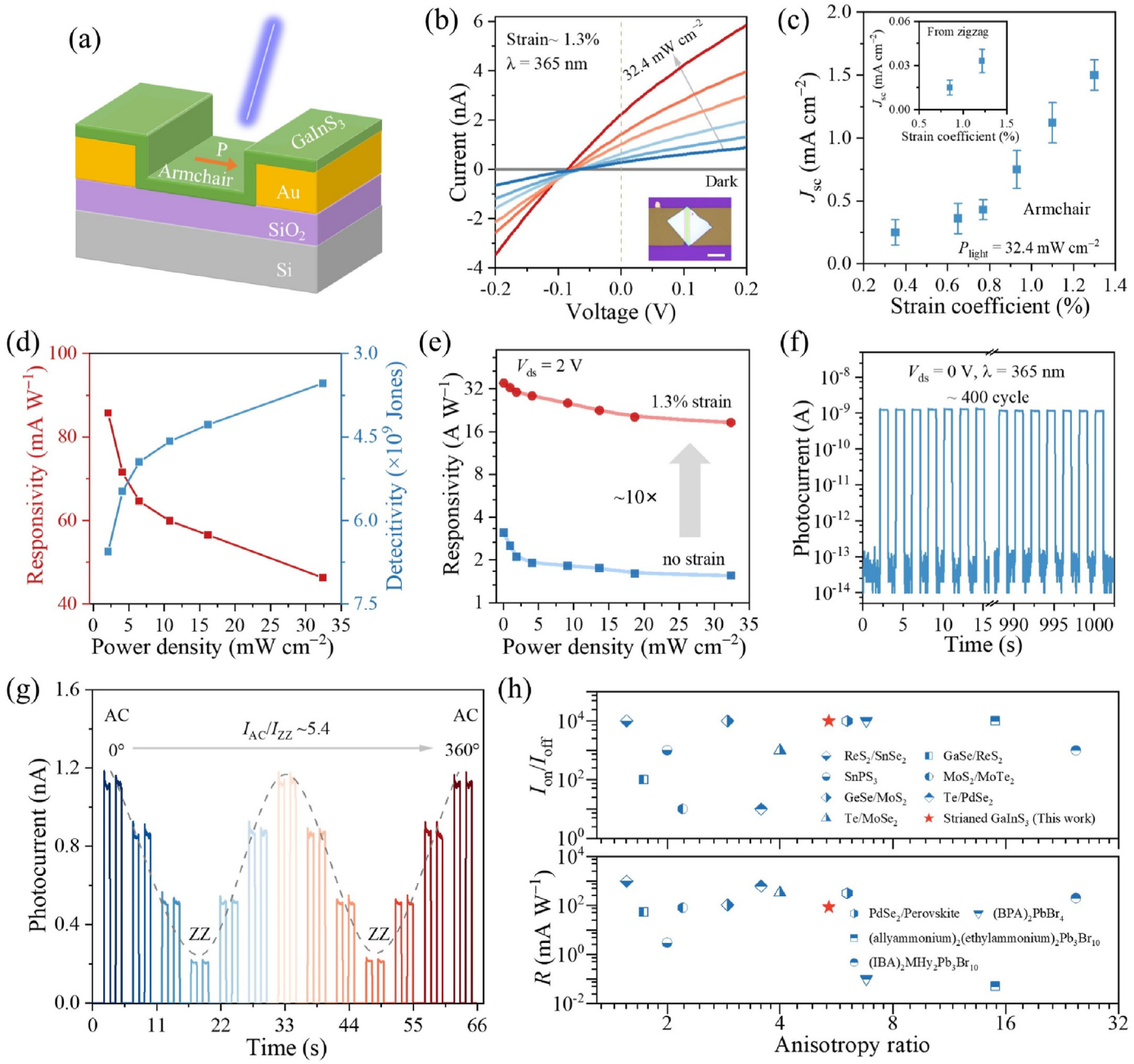

Fig. 4. The photovoltaic response of strained $GaInS_3$ device. (a) Schematic of the strained device. (b) The power-dependent *I-V* curve of $GaInS_3$ with 1.3 % strain at a wavelength of 365 nm. The inset is optical image of strained $GaInS_3$ device, scale bar: 10 μm. (c) The extracted short-circuit current density diagrams of different strain coefficients in the AC direction, with the inset depicting the strain in the ZZ direction. All J_{sc} is extracted from same incident light. (d) Power-density-dependent responsivity and detectivity under zero bias voltage. (e) Under the same wavelength and bias voltage, the power density-dependent responsivity curves of the 1.3 % strained device and the normal device. (f) Self-powered 400-cycle *I-T* curve of 1.3 % strained device at 365 nm light (power density: 16.2 mW cm^{-2}). (g) The measured photocurrent at the polarized angle ranging from 0° to 360° at the wavelength of 365 nm (power density: 16.2 mW cm^{-2}). The anisotropic ratio is ~5.4. (h) A statistical comparison chart of the device photoelectric performances (responsivity and I_{on}/I_{off}) of anisotropic 2D heterojunctions, ferroelectric and bulk ferroelectric materials.

light power. After fitting, the power function value of I_{shg} and P_{light} is equal to 2, precisely conforming to the second-order nonlinear optical theory [30]. SHG mapping is capable of directly observing crystallinity and phase uniformity of 2D nanosheets. As presented in Fig. 2c, the mapping of $GaInS_3$ vividly demonstrates the disparity in SHG intensities among nanoflakes of different thicknesses. In samples of the same thickness, a homogeneous SHG intensity is manifested. With the augmentation of thickness, the SHG intensity undergoes a remarkable enhancement. This indicates that the $GaInS_3$ nanosheets have outstanding crystallinity and that the dipole polarization accumulates along with the increase in thickness. Subsequently, as shown in Fig. 2d, we extracted the SHG intensities of $GaInS_3$ nanoflakes of different thicknesses and made a comparison with that of 1L 2H-MoS_2. When the thickness of $GaInS_3$ attains 10L, its second-harmonic intensity is equivalent to that of 1L MoS_2, that is to say, its SHG coefficient (χ^2) approximates to 0.1 times that of MoS_2. Owing to its inherent non-centrosymmetric structure, both odd- and even-numbered layers of $GaInS_3$ possess strong SHG intensity and enhance with the increase in thickness. Although 1L-MoS_2 [31], anisotropic SnS [32], and ReS_2 [33] also exhibit strong SHG responses, their SHG is highly contingent upon

the constraint of layer number. They can merely display symmetry breaking in odd or even layers, and the SHG intensity declines steeply or even vanishes as the layer number increases. In contrast to these types of materials, the intrinsic non-centrosymmetric structure does not necessitate complex and cumbersome operations for controlling the number of layers. The polarized SHG polar plot indicates the C_{2v} symmetry of $GaInS_3$ and can simultaneously determine its crystal orientation. Two-dimensional materials, owing to their large deformation tolerance, are conducive to regulating their physical properties via strain engineering [19,20,34]. To explore the mechanism of strain engineering on the $GaInS_3$ SHG response, we prepared strained $GaInS_3$ nanoflakes through mechanical exfoliation [35]. Based on the optical image in Fig. 2e, the contrast of the wrinkled $GaInS_3$ nanoflakes undergoes obvious changes. AFM is further employed to characterize the morphology and height of both normal and wrinkled nanoflakes (Fig. S7a). The strained $GaInS_3$ SHG mapping reveals a remarkable enhancement of the SHG intensity at the wrinkles, and the intensities in different regions are extracted for comparison. Based on the height and width of the wrinkles as well as the thickness of the nanosheet, the corresponding strain coefficient can be estimated [35]. As presented in Fig. 2f, the SHG intensity undergoes a significant enhancement with the increase of strain. Remarkably, the SHG intensity was enhanced by approximately 54 times compared to the original one at 1.2 % strain. The distinct variations of the SHG response prove that the dipole polarization in the $GaInS_3$ structure can be improved by strain engineering.

Piezoelectric materials typically require structures with anisotropic dipole moments that are non-centrosymmetric, thereby achieving the polarization of the materials [36,37]. Therefore, it is necessary to check the piezoelectric properties of $GaInS_3$ for analyzing its effect of in-plane polarization. The PFM is the most extensively employed means for verifying the piezoelectric phenomena of materials at the micro-nano scale [38,39]. As depicted in Fig. 3a, the conductive tip on the cantilever spring arm makes contact with the sample surface, and a variable excitation voltage is applied between the surface and the tip. Owing to the electro-strictive or expansion effect of piezoelectric materials, upon the application of a divining voltage, the sample surface undergoes deformation. Under the influence of the driving voltage, the sample surface will undergo deformation, and the laser will detect the positional change of the cantilever arm. After identification and conversion by the position sensitive detector and the phase-locked amplifier, the corresponding amplitude and phase signals are output in the computer. By regulating the contact mode of the cantilever arm in the vertical or lateral direction, the out-of-plane or in-plane polarization of the material can be gathered. For the analysis of the in-plane polarization of 2D $GaInS_3$, lateral PFM is employed to further measure its piezoelectric response. When DC voltage sweeps between −6 V and +6 V with an AC voltage of 2 V, the amplitude response curve exhibits a butterfly loop of approximately 1.3 V, and the phase undergoes a 180° switch at the same turning point (Fig. 3b). To further validate the piezoelectric response and extract the curve of voltage-dependent amplitude response, the in-plane amplitude and phase mapping of $GaInS_3$ nanosheets were collected under the driving voltages ranging from 1 V to 4 V, as depicted inFig. 3c and S8, respectively. As the voltage is gradually increased, distinct amplitude and phase contrast variations can be observed in $GaInS_3$, while the Si substrate is hardly change. Subsequently, we tested the amplitude responses of nanosheets of different thicknesses and fitted the linear slopes. As shown in Fig. 3d, with the increase in thickness, the lateral amplitude of $GaInS_3$ also gradually increases at the same voltage, and the extracted maximum slope is about 48 pm V^{-1}. These pieces of evidence indicate the robust in-plane piezoelectricity in 2D $GaInS_3$ and also offer support for us to enhance the spontaneous polarization through strain engineering.

It is widely acknowledged that 2D III−VI groups are a kind of classic

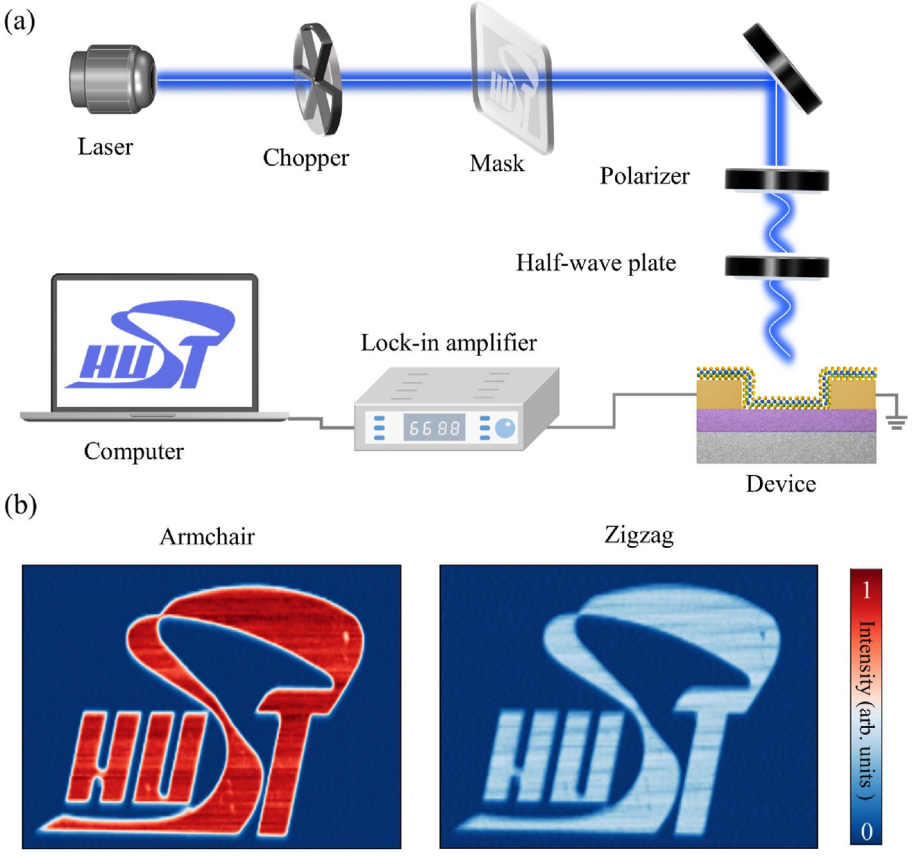

Fig. 5. Self-powered imaging of strained $GaInS_3$ device. (a) Schematic illustration of the imaging measurement system. (b) The imaging results of the strained device with polarized light along the AC and ZZ directions at a wavelength of 405 nm.

photoelectric semiconductors [40,41], and the photoelectric response of 2D $GaInS_3$ is also worthy of attention. As depicted in Fig. S9, since 2D $GaInS_3$ devices exhibit an obvious photoelectric response in the ultraviolet band, the incident laser of 365 nm was selected in this work to investigate the optoelectronic properties systematically. After testing and analysis, the $GaInS_3$ device showed excellent optoelectronic performance, such as a high I_{light}/I_{dark} ratio of ~10^6, a responsivity of ~2.5 A W^{-1}, and a large detectivity of 6.55×10^{10} Jones. The intrinsic in-plane anisotropic structure of $GaInS_3$ prompts further investigation on its polarized optoelectronic response. The $GaInS_3$ devices demonstrate a distinct angle-dependent photocurrent, with an extracted polarization ratio of approximately 1.72, which is comparable to the current 2D anisotropic photoelectric materials, such as SiP_2 [42], $NbOI_2$ [43], As_2S_3 [44], KNb_3O_8 [45]. In previous experiments, 2D $GaInS_3$ was verified to be a material featuring in-plane anisotropy, piezoelectricity, and photoelectric response. Consequently, we propose to enhance the in-plane polarization via strain engineering to achieve the photovoltaic effect of $GaInS_3$. Firstly, Au electrodes with a thickness ranging from 150 to 200 nm are evaporated on the 300 nm SiO_2/Si substrate. Secondly, the crystal orientation of the exfoliated $GaInS_3$ nanoflakes is determined by polarized Raman or SHG. Finally, the nanoflakes are transferred onto the bottom electrodes by the dry transfer method (Fig. 4a). Since the maximum photocurrent of 2D $GaInS_3$ is along the AC orientation, the strain-induced photoelectric response along the AC direction is mainly concerned without additional clarification. At $\lambda = 365$ nm, the light power-dependent *I-V* curve of $GaInS_3$ with a strain coefficient of 1.3 % was employed to analyze its photovoltaic response feature (Fig. 4b). When in the dark state, the strained $GaInS_3$ still maintains a dark current of less than pA, and it short-circuit current (I_{sc}) increases with the increase of the incident light power. When the power density of light is 32.4 mW cm^{-2}, open-circuit voltage (V_{oc}) is approximately −80 mV and I_{sc} reaches ~2.28 nA. Fig. 4c shows the strain coefficient-dependent densities of short-circuit current (J_{sc}) extracted to further analyze the relationship between strain and the photovoltaic response of $GaInS_3$. Under the same incident light power, when the strain coefficient increased from 0.35 % to 1.3 %, the J_{oc} also increased from 0.25 mA cm^{-2} to 1.5 mA cm^{-2}. This outperforms bulk photovoltaic crystals [46–48] and is comparable to the currently reported 2D bulk photovoltaic materials such as SnP_2Se_6 [49] and $CuInP_2S_6$ [18]. Additionally, in order to comprehend the mechanism of the polarization direction on the photovoltaic response of $GaInS_3$, we also compared the I_{sc} in the AC and ZZ directions. According to the inset of Fig. 4c, under the same conditions, the current subjected to strain along the ZZ direction undergoes a significant attenuation, only 2–3 % of the current in the AC direction. This distinct contrast demonstrates that the strain along the polarization-sensitive direction is vital for the photovoltaic response regulation in $GaInS_3$. In Fig. 4e, under the same V_{ds}, the photoresponsivity of $GaInS_3$ with a 1.3 % strain is enhanced by approximately one order of magnitude compared to the normal state. This also suggests that the photoelectric performance of $GaInS_3$ can be significantly improved through strain engineering. After 400 cycles, the strained device maintained outstanding stability with a high I_{on}/I_{off} ratio and no obvious decline of the photocurrent compared to the initial state (Fig. 4f), suggesting that the $GaInS_3$ device can achieve the enduring self-powered photodetectors. The strained device also exhibits a fast response speed (<40 ms, Fig. S12b). Strain engineering not only conspicuously enhances the optoelectronic performance of 2D materials but also has the potential to reduce the structure symmetry. Therefore, the research on the polarized photoelectric response of strained $GaInS_3$ device is conducive to our further verifying of this assumption. According to Fig. 4g, the photocurrent of the strained $GaInS_3$ device shows a distinct angle-dependent characteristic, with $I_{ph\text{-}max}$ and $I_{ph\text{-}min}$ corresponding to the AC direction and the ZZ direction, respectively. The polarization ratio extracted from the strained device is up to 5.4, which represents a remarkable increase compared to that of the previous normal device (~1.72). Based on the current reports of self-powered photodetectors of 2D heterojunctions [50–56], 2D or bulk ferroelectric materials [57–60], the strained $GaInS_3$ device demonstrates balance performance, such as a high I_{on}/I_{off} ratio (>10^4), a suitable responsivity (~85 mA W^{-1}), and a large polarization ratio (~5.4). As depicted in Fig. 5a, we employed an imaging test system to assess the application of the strained $GaInS_3$ device in self-powered imaging technology. Under a 455 nm light source, the strained device presents a "HUST" pattern with a remarkable contrast disparity at 0° and 90° of polarized light, which indicates that the device possesses self-powered polarization detection and imaging performance. Therefore, enhancing the in-plane polarization of the anisotropic piezoelectric $GaInS_3$ through strain engineering can facilitate its emergence as a promising candidate for self-powered detection and imaging devices.

4. Conclusion

In summary, we have confirmed that the in-plane polarization of the anisotropic piezoelectric $GaInS_3$ can be enhanced through strain engineering to achieve self-powered polarization-sensitive detection and imaging. The anisotropy of 2D $GaInS_3$ is verified through polarized Raman and reflectance difference spectroscopy, and the dipole polarization within the structure is analyzed by means of SHG and PFM. Strain is applied to enhance the in-plane polarization by transferring $GaInS_3$ nanosheets onto bottom electrodes with stepped heights, enabling the generation of photovoltaic responses. The strained device demonstrates outstanding self-powered polarization photoelectric detection and imaging performance, featuring a high I_{on}/I_{off} ratio (>10^4) and a large polarization ratio (~5.4). This work not only offers an anisotropic 2D piezoelectric material but also provides forward-looking guidance for the development of high-performance self-powered polarization-sensitive detection and imaging devices.

CRediT authorship contribution statement

Zongdong Sun: Writing – review & editing, Writing – original draft, Methodology, Conceptualization. **Jie Liu:** Methodology, Conceptualization. **Na Zhang:** Methodology, Conceptualization. **Wanfu Shen:** Methodology. **Chunguang Hu:** Methodology. **Liang Li:** Methodology. **Feng Yan:** Methodology. **Fangfang Xia:** Writing – review & editing, Methodology. **Huiqiao Li:** Writing – review & editing, Supervision, Project administration, Methodology. **Yuan Li:** Writing – review & editing, Methodology. **Tianyou Zhai:** Writing – review & editing, Writing – original draft, Supervision, Project administration, Methodology, Formal analysis, Conceptualization.

Declaration of competing interest

The authors declare that they have no known competing financial interests or personal relationships that could have appeared to influence the work reported in this paper.

Acknowledgements

This work was supported by the National Key R&D Program of China (2023YFE0210800), the National Natural Science Foundation of China (Nos. U21A2069 and 22350003), Shenzhen Science and Technology Program (Nos. JCYJ20240813153403005 and JCYJ20220818102215033), Guangdong Basic and Applied Basic Research Foundation (No. 2023B1515120041), the Innovation Project of Optics Valley Laboratory (No. OVL2023PY007), Guangdong HUST Industrial Technology Research Institute, and Guang-dong Provincial Key Laboratory of Manufacturing Equipment Digitization (No. 2023B1212060012). The authors also thank the characterization support from Analytical and Testing Center in Huazhong University of Science and Technology.

Appendix A. Supplementary data

Supplementary data to this article can be found online at https://doi.org/10.1016/j.tramat.2025.100009.

References

[1] W. Xin, W. Zhong, Y. Shi, Y. Shi, J. Jing, T. Xu, J. Guo, W. Liu, Y. Li, Z. Liang, X. Xin, J. Cheng, W. Hu, H. Xu, Y. Liu, Low-dimensional-materials-based photodetectors for next-generation polarized detection and imaging, Adv. Mater. 36 (2023) 2306772.

[2] J. Wang, C. Jiang, W. Li, X. Xiao, Anisotropic low-dimensional materials for polarization-sensitive photodetectors: from materials to devices, Adv. Opt. Mater. 10 (2022) 2102436.

[3] F. Wang, S. Zhu, W. Chen, J. Han, R. Duan, C. Wang, M. Dai, F. Sun, Y. Jin, Q.J. Wang, Multidimensional detection enabled by twisted black arsenic–phosphorus homojunctions, Nat. Nanotechnol. 19 (2024) 455–462.

[4] N.A. Rubin, G. D'Aversa, P. Chevalier, Z. Shi, W.T. Chen, F. Capasso, Matrix fourier optics enables a compact full-Stokes polarization camera, Science 365 (2019) eaax1839.

[5] K. Zou, K. Pang, H. Song, J. Fan, Z. Zhao, H. Song, R. Zhang, H. Zhou, A. Minoofar, C. Liu, X. Su, N. Hu, A. McClung, M. Torfeh, A. Arbabi, M. Tur, A.E. Willner, High-capacity free-space optical communications using wavelength- and mode-division-multiplexing in the mid-infrared region, Nat. Commun. 13 (2022) 7662.

[6] J.-B. Zhang, N. Zhou, L.-H. Zhang, C.-H. Shang, J.-X. Li, Y. Zhao, G.-H. Jia, R.-S. Yang, H. Xu, X.-B. Li, Optical and electrical anisotropy regulation engineering of low-dimensional materials toward polarized detection and imaging applications, Rare Met. 43 (2024) 2968–2993.

[7] Z. Li, T. Yan, X. Fang, Low-dimensional wide-bandgap semiconductors for UV photodetectors, Nat. Rev. Mater. 8 (2023) 587–603.

[8] C. Tan, X. Cao, X.J. Wu, Q. He, J. Yang, X. Zhang, J. Chen, W. Zhao, S. Han, G.H. Nam, M. Sindoro, H. Zhang, Recent advances in ultrathin two-dimensional nanomaterials, Chem. Rev. 117 (2017) 6225–6331.

[9] X. Wang, Y. Cui, T. Li, M. Lei, J. Li, Z. Wei, Recent advances in the functional 2d photonic and optoelectronic devices, Adv. Opt. Mater. 7 (2019) 1801274.

[10] Y. Ma, H. Yi, H. Liang, W. Wang, Z. Zheng, J. Yao, G. Yang, Low-dimensional van der Waals materials for linear-polarization-sensitive photodetection: materials, polarizing strategies and applications, Mater, Futures 3 (2024) 012301.

[11] L. Li, W. Han, L. Pi, P. Niu, J. Han, C. Wang, B. Su, H. Li, J. Xiong, Y. Bando, T. Zhai, Emerging in-plane anisotropic two-dimensional materials, InfoMat 1 (2019) 54–73.

[12] X. Li, H. Liu, C. Ke, W. Tang, M. Liu, F. Huang, Y. Wu, Z. Wu, J. Kang, Review of anisotropic 2d materials: controlled growth, optical anisotropy modulation, and photonic applications, Laser Photon. Rev. 15 (2021) 2100322.

[13] J. You, Z. Jin, Y. Li, T. Kang, K. Zhang, W. Wang, M. Xu, Z. Gao, J. Wang, J.K. Kim, Z. Luo, Epitaxial growth of 1D Te/2D $MoSe_2$ mixed-dimensional heterostructures for high-efficient self-powered photodetector, Adv. Funct. Mater. 34 (2023) 2311134.

[14] B. Zhang, Z. Ao, X. Lan, J. Zhong, F. Zhang, S. Zhang, R. Yang, L. Wang, P. Chen, G. Wang, X. Yang, H. Liu, J. Cao, M. Zhong, H. Li, Z. Zhang, Self-rolled-up WSe_2 one-dimensional/two-dimensional homojunctions: enabling high-performance self-powered polarization-sensitive photodetectors, Nano Lett. 24 (2024) 7716–7723.

[15] S. Kim, M. Kim, H. Kim, Self-powered photodetectors based on two-dimensional van der Waals semiconductors, Nano Energy 127 (2024) 109725.

[16] H. Qiao, Z. Huang, X. Ren, S. Liu, Y. Zhang, X. Qi, H. Zhang, Self-powered photodetectors based on 2d materials, Adv. Opt. Mater. 8 (2019) 1900765.

[17] D. Zhang, P. Schoenherr, P. Sharma, J. Seidel, Ferroelectric order in van der Waals layered materials, Nat. Rev. Mater. 8 (2023) 25–40.

[18] Y. Li, J. Fu, X. Mao, C. Chen, H. Liu, M. Gong, H. Zeng, Enhanced bulk photovoltaic effect in two-dimensional ferroelectric $CuInP_2S_6$, Nat. Commun. 12 (2021) 5896.

[19] X. Yu, Z. Peng, L. Xu, W. Shi, Z. Li, X. Meng, X. He, Z. Wang, S. Duan, L. Tong, X. Huang, X. Miao, W. Hu, L. Ye, Manipulating 2d materials through strain engineering, Small (2024) 2402561.

[20] J. Wang, L. He, Y. Zhang, H. Nong, S. Li, Q. Wu, J. Tan, B. Liu, Locally strained 2d materials: preparation, properties, and applications, Adv. Mater. (2024) 2314145.

[21] Y. Dong, M.-M. Yang, M. Yoshii, S. Matsuoka, S. Kitamura, T. Hasegawa, N. Ogawa, T. Morimoto, T. Ideue, Y. Iwasa, Giant bulk piezophotovoltaic effect in 3R-MoS_2, Nat. Nanotechnol. 18 (1) (2022) 36–41.

[22] W. Wang, Y. Xiao, T. Li, X. Lu, N. Xu, Y. Cao, Piezo-photovoltaic effect in monolayer 2H-MoS_2, J. Phys. Chem. Lett. 15 (2024) 3549–3553.

[23] J. Jiang, Z. Chen, Y. Hu, Y. Xiang, L. Zhang, Y. Wang, G.-C. Wang, J. Shi, Flexo-photovoltaic effect in MoS_2, Nat. Nanotechnol. 16 (2021) 894–901.

[24] Z. Sun, J. Liu, Y. Xu, X. Xiong, Y. Li, M. Wang, K. Liu, H. Li, Y. Wu, T. Zhai, Low-symmetry van der waals dielectric $GaInS_3$ triggered 2d MoS_2 giant anisotropy via symmetry engineering, Adv. Mater. 36 (2024) 2410469.

[25] W. Chen, H. Yin, S. Jiang, S. Liu, C. Liu, B. Wang, G.-P. Zheng, Anomalous layer-dependent electronic and piezoelectric properties of 2d $GaInS_3$ nanosheets, Appl. Phys. Lett. 118 (2021) 213103.

[26] S. Zhao, P. Luo, S. Yang, X. Zhou, Z. Wang, C. Li, S. Wang, T. Zhai, X. Tao, Low-symmetry and nontoxic 2D SiP with strong polarization-sensitivity and fast photodetection, Adv. Opt. Mater. 9 (2021) 2100198.

[27] R. Beams, L.G. Cancado, S. Krylyuk, I. Kalish, B. Kalanyan, A.K. Singh, K. Choudhary, A. Bruma, P.M. Vora, F. Tavazza, A.V. Da-Vydov, S.J. Stranick, Characterization of few-layer 1T′ $MoTe_2$ by polarization-resolved second harmonic generation and Raman scattering, ACS Nano 10 (2016) 9626–9636.

[28] W.J. Huang, Y. Xiao, F.F. Xia, X.B. Chen, T.Y. Zhai, Second harmonic generation control in 2d layered materials: status and outlook, Adv. Funct. Mater. 34 (2024) 2310726.

[29] A.R. Khan, L. Zhang, K. Ishfaq, A. Ikram, T. Yildrim, B. Liu, S. Rahman, Y. Lu, Optical harmonic generation in 2D materials, Adv. Funct. Mater. 32 (3) (2021) 2105259.

[30] A. Autere, H. Jussila, Y. Dai, Y. Wang, H. Lipsanen, Z. Sun, Nonlinear optics with 2d layered materials, Adv. Mater. 30 (2018) 1705963.

[31] N. Kumar, S. Najmaei, Q. Cui, F. Ceballos, P.M. Ajayan, J. Lou, H. Zhao, Second harmonic microscopy of monolayer MoS_2, Phys. Rev. B 87 (2013) 161403.

[32] M. Zhu, M. Zhong, X. Guo, Y. Wang, Z. Chen, H. Huang, J. He, C. Su, K.P. Loh, Efficient and anisotropic second harmonic generation in few-layer SnS film, Adv. Opt. Mater. 9 (2021) 2101200.

[33] J. Wang, N.N. Han, Z.D. Luo, M.W. Zhang, X.Q. Chen, Y. Liu, Y. Hao, J.L. Zhao, X.T. Gan, Electrically tunable second harmonic generation in atomically thin ReS_2, ACS Nano 16 (2022) 6404–6413.

[34] Y. Qi, M.A. Sadi, D. Hu, M. Zheng, Z. Wu, Y. Jiang, Y.P. Chen, Recent progress in strain engineering on van der waals 2d materials: tunable electrical, electrochemical, magnetic, and optical properties, Adv. Mater. 35 (2023) 2205714.

[35] S. Rahman, T. Yildirim, M. Tebyetekerwa, A.R. Khan, Y. Lu, Extraordinary nonlinear optical interaction from strained nanostructures in van der waals $CuInP_2S_6$, ACS Nano 16 (2022) 13959–13968.

[36] P.C. Sherrell, M. Fronzi, N.A. Shepelin, A. Corletto, D.A. Winkler, M. Ford, J.G. Shapter, A.V. Ellis, A bright future for engineering piezoelectric 2d crystals, Chem. Soc. Rev. 51 (2022) 650–671.

[37] Q. Zhang, S. Zuo, P. Chen, C. Pan, Piezotronics in two-dimensional materials, InfoMat 3 (2021) 987–1007.

[38] X. Jiang, X. Zhang, R. Niu, Q. Ren, X. Chen, G. Du, Y. Chen, X. Wang, G. Tang, J. Lu, X. Wang, J. Hong, Strong piezoelectricity and improved rectifier properties in mono- and multilayered $CuInP_2S_6$, Adv. Funct. Mater. 33 (2023) 2213561.

[39] W.F. Io, M.-C. Wong, S.-Y. Pang, Y. Zhao, R. Ding, F. Guo, J. Hao, Strong piezoelectric response in layered $CuInP_2S_6$ nanosheets for piezoelectric nanogenerators, Nano Energy 99 (2022) 107371.

[40] Z. Yang, J. Hao, Recent Progress in 2D Layered III–VI Semiconductors and their heterostructures for optoelectronic device applications, Adv. Mater. Technol. 4 (2019) 1900108.

[41] H. Cai, Y. Gu, Y.-C. Lin, Y. Yu, D.B. Geohegan, K. Xiao, Synthesis and emerging properties of 2D layered III–VI metal chalcogenides, Appl. Phys. Rev. 6 (2019) 041312.

[42] Z. Wang, P. Luo, B. Han, X. Zhang, S. Zhao, S. Wang, X. Chen, L. Wei, S. Yang, X. Zhou, S. Wang, X. Tao, T. Zhai, Strong in-plane anisotropic SiP_2 as a IV–V 2d semiconductor for polarized photodetection, ACS Nano 15 (2021) 20442–20452.

[43] Y. Fang, F. Wang, R. Wang, T. Zhai, F. Huang, 2D $NbOI_2$: a chiral semiconductor with highly in-plane anisotropic electrical and optical properties, Adv. Mater. 33 (2021) 2101505.

[44] M. Siskins, M. Lee, F. Alijani, M.R. van Blankenstein, D. Davidovikj, H.S.J. van der Zant, P.G. Steeneken, Highly anisotropic mechanical and optical properties of 2d layered As_2S_3 membranes, ACS Nano 13 (2019) 10845–10851.

[45] Y. Ping, H. Long, H. Liu, C. Chen, N. Zhang, H. Jing, J. Lu, Y. Zhao, Z. Yang, W. Li, F. Ma, X. Fang, Z. Wei, H. Xu, Polarization sensitive solar-blind ultraviolet photodetectors based on ultrawide bandgap KNb_3O_8 nanobelt with fringe-like atomic lattice, Adv. Funct. Mater. 32 (2022) 2111673.

[46] Z. Xiao, Y. Yuan, Y. Shao, Q. Wang, Q. Dong, C. Bi, P. Sharma, A. Gruverman, J. Huang, Giant switchable photovoltaic effect in organometal trihalide perovskite devices, Nat. Mater. 14 (2015) 193–198.

[47] S.Y. Yang, J. Seidel, S.J. Byrnes, P. Shafer, C.H. Yang, M.D. Rossell, P. Yu, Y.H. Chu, J.F. Scott, J.W. Ager, L.W. Martin, R. Ramesh, Above-bandgap voltages from ferroelectric photovoltaic devices, Nat. Nanotechnol. 5 (2010) 143–147.

[48] P.S. Brody, High voltage photovoltaic effect in barium titanate and lead titanate-lead zirconate ceramics, J. Solid State Chem. 12 (1975) 193–200.

[49] V.K. Sangwan, D.G. Chica, T.C. Chu, M. Cheng, M.A. Quintero, S.Q. Hao, C.E. Mead, H. Choi, R. Zu, J. Sheoran, J.Y. He, Y.K. Liu, E. Qian, C.C. Laing, M.A. Kang, V. Gopalan, C. Wolverton, V.P. Dravid, L.J. Lauhon, M.C. Hersam, M.G. Kanatzidis, Bulk photovoltaic effect and high mobility in the polar 2d semiconductor SnP_2Se_6, Sci. Adv. 10 (2024) eado8272.

[50] Z. Fu, J. Han, L. Wei, Y. Wei, X. Huo, C. Li, J. Xie, H. Zhou, H. Yu, J. Gou, Z. Wu, J. Wang, Polarization-sensitive self-powered photodetector based on anisotropic/isotropic $ReS_2/SnSe_2$ van der waals heterojunction, Adv. Opt. Mater. 12 (2024) 2401306.

[51] S. Quan, S. Guo, D. Weller, S. Fu, Y. Wang, R. Liu, Air-stable GaSe/ReS_2 heterojunctions for self-powered polarization-sensitive photodetectors, ACS Appl. Nano Mater. 5 (2022) 7365–7372.

[52] L. Kong, G. Li, Q. Su, X. Tan, X. Zhang, Z. Liu, G. Liao, B. Sun, T. Shi, Polarization-sensitive, self-powered, and broadband semimetal $MoTe_2/MoS_2$ van der waals heterojunction for photodetection and imaging, ACS Appl. Mater. Interfaces 15 (2023) 43135–43144.

[53] Y. Xin, X. Wang, Z. Chen, D. Weller, Y. Wang, L. Shi, X. Ma, C. Ding, W. Li, S. Guo, R. Liu, Polarization-sensitive self-powered type-II GeSe/MoS_2 van der waals heterojunction photodetector, ACS Appl. Mater. Interfaces 12 (2020) 15406–15413.

[54] P. Wang, Z. Li, X. Xia, J. Zhang, Y. Lan, L. Zhu, Q. Ke, H. Mu, S. Lin, Anisotropic Te/$PdSe_2$ van der waals heterojunction for self-powered broadband and polarization-sensitive photodetection, Small 20 (2024) 2401216.

[55] J. You, Z. Jin, Y. Li, T. Kang, K. Zhang, W. Wang, M. Xu, Z. Gao, J. Wang, J.-K. Kim, Z. Luo, Epitaxial growth of 1D Te/2D $MoSe_2$ mixed-dimensional heterostructures

for high-efficient self-powered photodetector, Adv. Funct. Mater. 34 (2024) 2311134.
[56] L.-H. Zeng, Q.-M. Chen, Z.-X. Zhang, D. Wu, H. Yuan, Y.-Y. Li, W. Qarony, S.P. Lau, L.-B. Luo, Y.H. Tsang, Multilayered $PdSe_2$/Perovskite Schottky Junction for Fast, Self-powered, polarization-sensitive, broadband photodetectors, and image sensor application, Adv. Sci. 6 (2019) 1901134.
[57] D. Li, J.-K. Qin, B. Zhu, L.-Q. Yue, P.-Y. Huang, C. Zhu, F. Zhou, L. Zhen, C.-Y. Xu, Intercorrelated ferroelectricity and bulk photovoltaic effect in two-dimensional $Sn_2P_2S_6$ semiconductor for polarization-sensitive photodetection, ACS Nano 18 (2024) 9636–9644.
[58] C. Ji, D. Dey, Y. Peng, X. Liu, L. Li, J. Luo, Ferroelectricity-driven self-powered ultraviolet photodetection with strong polarization sensitivity in a two-dimensional halide hybrid perovskite, Angew. Chem. Int. Ed. 59 (2020) 18933–18937.
[59] Y. Peng, X. Liu, Z. Sun, C. Ji, L. Li, Z. Wu, S. Wang, Y. Yao, M. Hong, J. Luo, Exploiting the bulk photovoltaic effect in a 2d trilayered hybrid ferroelectric for highly sensitive polarized light detection, Angew. Chem. Int. Ed. 59 (2020) 3933–3937.
[60] R. Li, Z. Wang, T. Zhu, H. Ye, J. Wu, X. Liu, J. Luo, Stereochemically active lone pair induced polar tri-layered perovskite for record-performance polarized photodetection, Angew. Chem. Int. Ed. 62 (2023) e202308445.